atmosphere

MDPI

Article

Evolution of Ozone above Togo during the 1979–2020 Period

Koffi Ayassou [1,2,*], Andrea Pazmiño [1], Kokou Sabi [2], Ariane Bazureau [1] and Sophie Godin-Beekmann [3]

[1] LATMOS, UVSQ Université Paris Saclay, CNRS, 78280 Guyancourt, France
[2] LCA, Université de Lomé, Lomé BP 1515, Togo
[3] LATMOS, Sorbonne Université, CNRS, 75005 Paris, France
* Correspondence: koffi.ayassou@latmos.ipsl.fr or ayass91@yahoo.fr

Abstract: The objective of this paper is to estimate the trend of the Total Ozone Column (TOC) over Togo. A Multi-Sensor Reanalysis-2 (MSR-2) of the TOC over the entire territory of Togo was used. A Multiple Linear Regression (MLR) method has been applied to retrieve the interannual contributions of different forcings and the long-term variability. It was found that the Annual Oscillation (AnO), the Quasi Biennial Oscillation at 30 mb (QBO30), the Solar Flux (SF), and the El Niño–Southern Oscillation (ENSO) has a statistically significant influence on the interannual variability of the TOC. The strongest contribution (22 ± 1.4 DU) is allocated to the AnO while the weakest (<1 DU) is attributed to the Semi-Annual Oscillations (SAnO). Before the peak year of the Equivalent Effective Stratospheric Chlorine (EESC) in the tropics in 1997, the trend is negative (−0.3% ± 0.9% per decade) and is not statistically significant. After the peak year, a statistically significant positive trend is observed. The trend of the TOC is 0.6% ± 0.2% per decade. The monthly TOC trend over Togo is positive and statistically significant during the rainy season (particularly during the monsoon period) except in April, unlike during the harmattan period (DJF), where the trend is not significant.

Keywords: ozone; MLR; Togo; MSR-2; total column ozone; trend

Citation: Ayassou, K.; Pazmiño, A.; Sabi, K.; Bazureau, A.; Godin-Beekmann, S. Evolution of Ozone above Togo during the 1979–2020 Period. *Atmosphere* **2022**, *13*, 2066. https://doi.org/10.3390/atmos13122066

Academic Editor: Yoshihiro Tomikawa

Received: 22 October 2022
Accepted: 5 December 2022
Published: 8 December 2022

1. Introduction

Stratospheric ozone plays an essential role in sustaining life on earth by filtering the most energetic solar ultra-violet (UV) radiation. Prolonged exposure without protection to these UV radiations causes serious health risks (e.g., skin cancer) [1] and also affects biodiversity, especially crops and the marine ecosystem [2,3]. Given this important role played by the stratospheric ozone, it is, therefore, necessary to regularly monitor its evolution. Ozone is produced more in the tropical zone and is transported to extratropical zones by the Brewer–Dobson Circulation (BDC) [4–6].

The balance of the stratospheric ozone is influenced by chemical, dynamic, and radiative processes. Important ozone depletion was observed until the mid-1990s, followed by a stabilization of the ozone layer [7–12]. Ozone-depleting substances (ODS) are responsible for this increased depletion. They are organic halogen compounds of anthropogenic origin used in many sectors, including refrigeration, air conditioning, foam inflation, the cleaning of electronic components, and as solvents [13,14]. To protect the ozone layer and prevent its depletion, the international community set up the Vienna Convention for the protection of the ozone layer, adopted on 22 March 1985, under the aegis of the United Nations, and the Montreal Protocol for the regulation of ODS, which was signed on 16 September 1987, and entered into force in 1989. This Protocol aims to gradually reduce the production and use of ODS and their releases into the atmosphere in order to bring the ozone layer back to its 1980 reference levels [15]. According to the many assessments on the state of the ozone layer that were published after the signature of the Montreal Protocol (e.g., WMO, 2018 [16], the most recent one), the trends of the TOC in the tropics before and after the peak of halogen loading in the stratosphere, which occurred around 1995–1997, depending on the altitude in the midlatitude and tropical regions [17,18], are low compared

to those in the extratropical zones [19]. Recent studies also showed a continuous decrease in ozone in the tropical and midlatitudes lower stratosphere after the ODS peak that is not simulated by chemistry-climate models [20,21]. Furthermore, Coldewey-Egbers et al. [22] found a non-significant trend in the TOC in the tropics from GOME-type Total Ozone Essential Climate Variable (GTO-ECV) data which combines total ozone observations from six satellite sensors with GOME-type nadir vision. The authors reported that this trend is likely to be related to the results of opposite trends in tropospheric and stratospheric partial columns [23,24].

Ozone total content is monitored worldwide with ground-based observation instruments. However, in western sub-Saharan Africa, and particularly in Togo, ground-based instruments are lacking. Consequently, the evaluation of trends in the long-term evolution of total ozone above Togo, together with the contribution of dynamic and radiative forcings of the trends, requires the use of satellite data. Some studies were conducted using available ground-based data in other tropical regions or with satellite data, but most used zonal averages [20–22,25].

Togo is a West African country located in the intertropical zone between 6° N and 11° N, and between 0°14′ W and 1°65′ E. Being a stakeholder in the Montreal Protocol, Togo has made commitments not only to reduce ODS emissions, but also to undertake ozone layer observation activities according to its supporting funders. So, the main objective of this study is to characterize the long-term trend of the TOC over Togo. Specifically, it aims to (a) determine the contribution of dynamic and other major forcings of the interannual and decadal variability of the TOC, (b) estimate the trend of the Total Ozone Column (TOC) over Togo, and (c) study the behavior of the TOC trend during the monsoon and harmattan periods. The 1979–2020 period is chosen because it corresponds to the stratospheric ozone depletion and stabilization period. Additionally, the time series corresponds to a moment when the planet is experiencing a phenomenon of global warming caused by the anthropogenic increase in Greenhouse Gas (GHG) emissions and, therefore, warming of the troposphere which, in turn, cools the stratosphere [26]. Our study is based on the use of the Multi Sensor Reanalysis-2 (MSR-2) ozone record. MSR-2 data were chosen because they are a gridded dataset allowing the collection of data specific to the territory of Togo. For the trend evaluation, we use a multilinear regression method that has been widely used for the analysis of the interannual and long-term contributions on total ozone datasets, the MLR method [25,27–29].

The structure of the paper is as follows. In Section 2, the data used are presented. In Section 3, the methodology applied in this study is presented. The analysis of ozone over Togo is described in Section 4 to determine the contribution of different forcings and trends since 1997, and the monthly trends of ozone according to the monsoon and harmattan periods in Togo. Finally, the conclusion of the study is presented in Section 5.

2. Data

In order to study the interannual and long-term variability of the TOC over Togo, a multilinear regression method was applied to MSR-2 total ozone [30] data covering the period 1979–2020.

MSR-2 ozone data are built on the basis of fourteen (14) satellite data sets [30]. Positioned in polar orbit, the 14 satellites measure in the Huggins UV band (305–340 nm). The first step in data construction is to apply error bias correction to the 14 satellite datasets based on total ozone column measurements from the TOC ground-based and UV measurement stations. The correction is made according to the solar zenith angle (SZA), viewing zenith angle (VZA), effective stratospheric temperature, time, and offset (with the year 2000 as a reference). The second step is to apply the data assimilation method to satellite datasets to create global ozone data. The assimilation method is that of the sub-optimal implementation of the Kalman filter technique based on the chemistry-transport model, TM3-DAM, which gives detailed information on the transport and chemistry of ozone in the stratosphere in order to assimilate the data. The data thus constructed are the im-

proved and extended version of MSR called MSR-2 and they are useful for studies of the TOC in places where measurement stations are lacking, such as in Africa, in particular in Togo. The spatial resolution of the data is 0.5° × 0.5° [31] and corresponds to ozone columns in the Dobson Unit (DU). MSR-2 data were chosen for this study because there is the possibility of extracting data specific to the Togolese national territory, unlike zonal data. These data have been used to study the trend of total ozone in the southern hemisphere and the Antarctic [9,28]. The data collected are monthly average values and cover 1979–2020 (Figure 1).

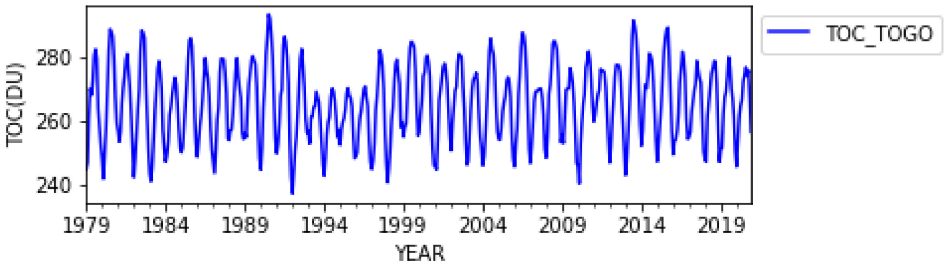

Figure 1. The monthly total ozone column over Togo from 1979–2020.

These data cover the national territory with latitudes between 6° and 11° N, and longitudes between 0°14′ W and 1°65′ E. They were downloaded from the website of the tropospheric emissions monitoring service (TEMIS) of ESA/KNMI at the following address: https://www.temis.nl/protocols/o3total.php (accessed on 17 September 2021).

3. Methodology

The multilinear regression (MLR) method was applied to study the interannual variability and trend of the TOC over Togo. The MLR method used in this work is similar to that used in previous works [25,27,28]. The method was applied using the R statistical software [32]. It is appropriate for this study because it allows an explanation of ozone monthly means y_i by a linear relationship involving variables or dependent variables representing the different proxies $x_i^1, \ldots, x_i^p$ that are the so-called explanatory variables or control variables. The proxies are considered independent and endogenous. For an explained variable, the y_i is written in the following form:

$$y_i = \beta_0 + \beta_1 x_i^1 + \beta_2 x_i^2 + \ldots + \beta_P x_i^p + \varepsilon_i \quad (1)$$

where i = 1, 2, 3, … … n denotes the months of temporal series, β_0, β_1, … , β_P are the coefficients to be estimated, and ε_i is the error or residuals of the model expressing the missing information in the explanation of y_i by $x_i^1, \ldots, x_i^p$. The method is valid if the residuals are not autocorrelated. In order to take this into account, the autocorrelation of the residuals, the Cochrane–Orcutt transformation was applied [33] to the MLR method thanks to the Rcommender (Rcmdr) library and the package Orcutt of R statistical software, allowing us to have a valid MLR model.

The equation of the MLR method used is schematized by the following relation:

$$\begin{aligned} Y(t) = K + C_{QBO30}QBO30(t) + C_{QBO10}QBO10(t) + C_{ENSO}ENSO(t) + \\ C_{SF}SF(t) + C_{AnO}AnO(t) + C_{SAnO}SAnO(t) + C_{T1}T1(t) + C_{T2}T2(t) + \in (t) \end{aligned} \quad (2)$$

where

- Y(t) is the monthly TOC average,
- t designates the month between 1 and 504, i.e., the number of months between 1979 and 2020,
- K denotes the constant (intercepts) of the model,
- Cproxy designates the regression coefficients of different proxies, and
- ∈ (t) is the total of the residuals of the ozone anomalies.

The regression coefficients have the same unit as the Y (t). Each proxy except T1, T2, the AnO, and SAnO was divided by its amplitude (Max-Min) which allowed for the standardized proxies to be introduced into the model. This operation is called the standardization of proxies.

In this equation:

- The explained variable is the monthly average TOC for the time series and constitutes the input value of the MLR; and
- The explanatory variables are the Annual Oscillation (AnO), the Semi-Annual Oscillation (SAnO), the anomalies of the Solar Flux (SF), the El Niño–Southern Oscillation (ENSO), the Quasi-Biennial Oscillation at 30 mb (QBO30), the Quasi-Biennial Oscillation at 10 mb (QBO10), and the linear trend functions (T1; T2). The QBO, ENSO, and SF explanatory variables linked to the contribution of dynamical and radiative processes on total ozone interannual variability are the usual ones already used in different studies [22,34].

The AnO term corresponds to the annual variation of ozone and the SAnO term to the semiannual variation. The AnO is at the origin of the annual variation of ozone and both the AnO and SAnO act on the ozone according to the altitude and the periods of equinoxes and solstices. Their indices are defined by the following functions:

$$AnO = \cos\left(\frac{2\pi t}{12} + \frac{2\pi I}{180}\right) \text{ and } \quad SAnO = \sin\left(\frac{2\pi t}{6} + \frac{2\pi I}{180}\right) \tag{3}$$

where

- t is the rank of the months in the time series, and
- I is the phasing coefficient between the TOC time signal and the AnO or SanO.

In this study, I is set at −15 to simulate the AnO from the climatological TOC MSR-2 data (Figure 2a).

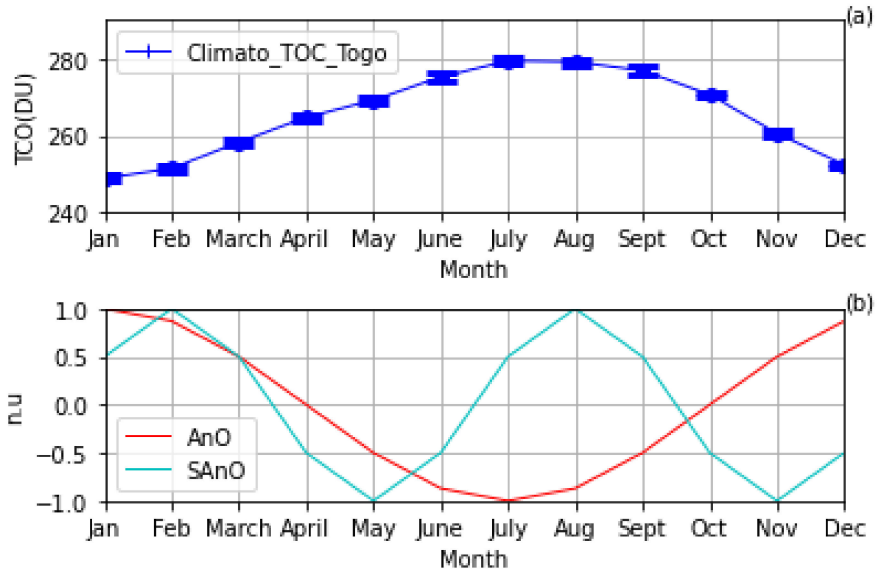

Figure 2. Climatology of the TOC (**a**) and the estimated proxies corresponding to the AnO and SAnO (Equation (1)) to simulate the climatology of the TOC (**b**) in the DU above Togo. The TOC is in the DU while the AnO and SAnO are in non-units (n.u).

The QBO is manifested in the tropical stratosphere by an inversion of zonal winds with descending cycles in an average period of 28 months. It thus has significant impacts on the global circulation of the atmosphere. The QBO30 is used in these works because it influences ozone variability in the tropics and mid-latitudes [34–37]. The QBO30 is

combined with the QBO10 to optimize the phase contribution of the QBO. Their indices are shown in Figure 3a.

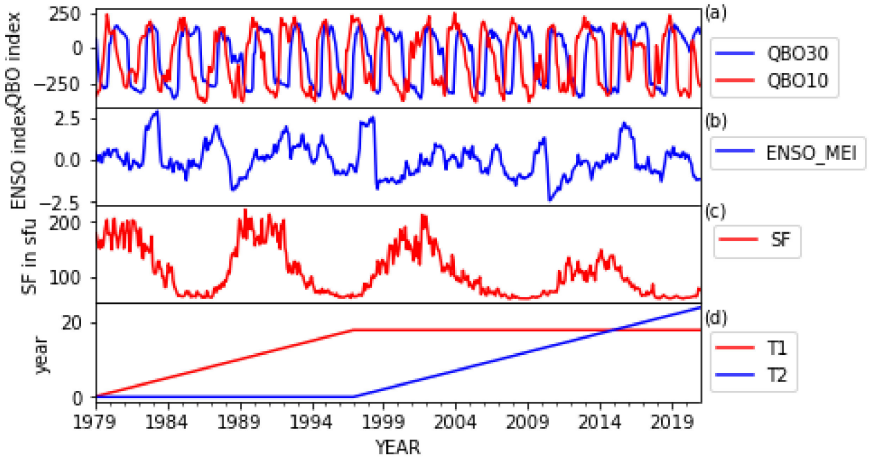

Figure 3. The Quasi-biennial Oscillation at 30 mb (QBO30) and 10 mb (QBO10) index (**a**), multivariate ENSO index version 2 (**b**), the Solar Flux (SF) index at a 10.7 cm wavelength in the SFU (Solar Flux Unit) with 1 $sfu = 10^{-22}.\mathrm{m}^{-2}.\mathrm{Hz}^{-1}$ (**c**), and trend functions T1 and T2 (see Equation (3)) as a function of the year (**d**).

The indices of ENSO forcing are represented in Figure 3b. The ENSO influences the change in atmospheric circulation by reinforcing these positive and negative anomalies in ocean surface temperatures [38,39]. This results in the reinforcement of the transport of ozone towards the subtropics, leading to a decrease in ozone in the east of the Pacific and an increase in the west [40,41]. In these works, the MEI (Multivariate ENSO Index) indices of ENSO are used [34,42,43].

Regarding the Solar Flux, it measures the variation of solar activity that influences the ozone content. The SF at a 10.7 cm wavelength is used [28,34,43,44] and is represented in Figure 3c.

According to Labitzke et al. and Gray et al. [45,46], the ozone balance is influenced by the variation in the activity of the sun through the radiative and photochemical forcing that it induces [47].

The two linear functions T1 and T2 (Figure 3d) represent the trend for the period before and after the turnaround year around 1997, corresponding with the peak of the EESC. As an approximation, they are represented by a linear function of time and considered as piecewise linear trends (PWLT) with the year of change set in 1997 [17,18,29,37,48], as seen below:

$$\mathrm{T1} = \begin{cases} \frac{\mathrm{t}}{12} & 0 < \mathrm{t} \leq \mathrm{T}_0 \\ \mathrm{T}_0 & \mathrm{T}_0 < \mathrm{t} \leq \mathrm{T}_{\mathrm{end}} \end{cases} \text{ and } \mathrm{T2} = \begin{cases} 0 & 0 < \mathrm{t} \leq \mathrm{T}_0 \\ \frac{(\mathrm{t}-\mathrm{T}_0)}{12} & \mathrm{T}_0 < \mathrm{t} \leq \mathit{Tend} \end{cases} \quad (4)$$

where T_0 is the last month of the year preceding the year in which the EESC started by decreasing, which corresponds to the month of December 1996 (the 216th month of the time series), and Tend to the last month of the series (the 504th month). The proxy for the trend is expressed in "year" and the regression coefficient in DU per year.

The sources of the other proxies apart from T1, T2, the AnO, and SAnO are presented in Table 1.

Table 1. Proxies used in this paper are present in column 1 and the corresponding sources and characteristics are in columns 2 and 3, respectively.

Proxy	Source	Characteristics
QBO 30 and 10	Freie Universität Berlin Department of Earth Sciences/Institute of Meteorology/Atmospheric Dynamics https://www.geo.fu-berlin.de/met/ag/strat/produkte/qbo/qbo.dat accessed on 22 September 2021	Monthly mean quasi-biennial oscillation at 30 mb and 10 mb
ENSO_MEI	NOAA Physical Science Laboratory https://psl.noaa.gov/enso/mei/data/meiv2.data accessed on 17 September 2021	Monthly average of the Multivariate ENSO Index Version 2
SF	The National Research Council of Canada Dominion Radio Astrophysical Observatory in Penticton ftp://ftp.geolab.nrcan.gc.ca/data/solar_flux/monthly_averages/solflux_monthly_average.txt ftp://ftp.seismo.nrcan.gc.ca/spaceweather/solar_flux/monthly_averages/solflux_monthly_average.txt both accessed on 25 November 2021	Monthly averages of Solar Flux at a 10.7 cm wavelength

To make the methodology used in this study more understandable, it is presented in the form of a flowchart (Figure A1).

4. Results and Discussion

4.1. Evaluation of the MLR Model

With the Cochrane–Orcutt transformation, the autocorrelation coefficient of the MLR model is ~0.2. This value of the autocorrelation coefficient is close to zero, showing a negligible autocorrelation between the residuals and thus making the model more robust and, therefore, applicable.

The relevance of the values of the coefficients will be validated on the basis of the value of the adjusted R^2 coefficient of determination, which should be close to 100%, and the *p*-value of the model, which should be less than 0.05.

The adjusted R^2 which takes into account the explanatory variables (proxies) and which gives the percentage of the variability explained by the model after the Cochrane–Orcutt transformation is 75%, which is close to 100%. The model after the Cochrane–Orcutt transformation explains 75% of the variability of the TOC over Togo. Similarly, the *p*-value of the model is much less than 0.01 (Table 2).

Table 2. General characteristics of the model.

R2	R2 Adjusted	p-Value
76%	75%	$<5.37 \times \mathrm{Exp}(-147)$

Several diagnostic tests were carried out using R software to show the robustness of the model. Indeed, the residual vs. fitted values test, which shows if residuals have a non-linear pattern, has allowed us to confirm that the model seems to be adapted because the residuals do not present a linear relationship with the simulated values. Additionally, the scale location, which is used to check the homogeneity of the variance of the residuals, showed that the variance of the residuals in our model is homogeneous. Moreover, the residuals of the model are more or less normally distributed around zero according to normality tests (e.g., Normal Q-Q), which shows that residuals are normally distributed. Likewise, there are no extreme values that can influence the results of the regression when

they are included or excluded according to the test of residual vs. leverage, which helps to find influential cases.

The MLR model uses the same dynamical and radiative forcings as those of the Trend-Run used by Toihir et al. [34], except the QBO10. It is different from that used by Weber et al. [25] in the sense that the proxies used are not the same and the year of the peak of the EESC considered here is 1997, whereas it is 1995 for the model used by them. Indeed, in their first model, they used two aerosol terms (Mt. Pinatubo 1992 and El Chichón 1983), the solar cycle term, the QBO10, the QBO50, and the ENSO, apart from the two independent linear trend terms. In the second version of their model, they included the Arctic Oscillation (AO), the Antarctic Oscillation (AAO), and the BDC (100 hPa eddy fluxes in the Northern and Southern Hemisphere). Otherwise, our model is different from the LOTUS (Long-term Ozone Trends and Uncertainties in the Stratosphere) model which is written in Python language and makes it possible to evaluate the trend of the vertical profile of ozone [49].

In view of the previous discussion, the model resulting from the Cochrane–Orcutt transformation is adapted to estimate the contribution of proxies, thus showing the quality of the results of the contributions of the forcings and the trend obtained. The uncertainty of the results is provided by error bars at two sigma.

4.2. Ozone above Togo

The regression coefficients, the contributions in absolute value, and the percentage of the forcings after model applications are summarized in Table 3.

Table 3. Regression coefficients and contributions of the forcings.

Proxies	**AnO**	**SAnO**	**QBO 30**	**QBO10**	**SF**	**ENSO**
Regression coefficients in the DU	-15.38 ± 0.71	0.59 ± 0.71	9.39 ± 0.29	0.98 ± 0.31	6.62 ± 0.17	-5.22 ± 0.18
Contributions to the DU	21.84 ± 1.42 ***	0.84 ± 1.42	5.35 ± 0.57 ***	0.60 ± 0.61	2.25 ± 0.34 ***	1.88 ± 0.36 ***
Contribution in %	67	3	16	2	7	6

*** Statistically significant at >2 sigma.

It should be noted in this table that the standard deviation error of the regression coefficient for the SanO is higher than the mean. This could be due to the fact that the SnAO acts on ozone according to altitude and, therefore, would influence the vertical profile of ozone more than the TOC over Togo.

The contribution of the different forcings was estimated by the formula $C_X * 2\sigma_x$, where C_x is the regression coefficient of the forcings noted X and σ_x designates the standard deviation of the time series of each normalized forcings [50].

According to Table 3, the SAnO (0.84 ± 1.42 DU) and the QBO10 (0.60 ± 0.61 DU) do not have a significant contribution to the TOC above Togo.

4.3. Contributions of Different Proxies

In absolute value, according to Table 3 and Figure 4, the strongest significant contribution is given by the AnO (21.84 ± 1.42 DU), as expected, while the smallest is given by the SAnO (0.84 ± 1.42 DU). In fact, the AnO characterizes the mechanism reflecting the seasonal variations of weather and climate. The contribution of the AnO is followed by that of the QBO30. After the QBO30, the forcing that controls the variability of the TOC is the SF. The ENSO contribution follows that of the Solar Flux.

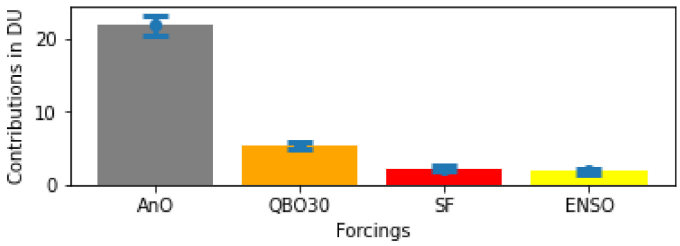

Figure 4. Significant forcings contribution at 2σ, indicated by the error bars.

This result obtained is consistent with that obtained by Zerefos et al. [51], who showed that if the contributions of the other proxies, i.e., those of the AnO, the QBO, and the SF are removed from the TOC time signal in tropical areas, a significant part would be explained by the ENSO. It is also in line with that obtained by Poulain et al. [52], who found that the interannual variability of the TOC is contributed by about 20% by the QBO and 5 to 20% by the ENSO in the tropics since in our study. Additionally, 18% (close to 20%) of the contribution is given by the QBO (QBO30 and 10) and 6% is given by the ENSO (Table 3).

4.4. Interannual Trends

The regression coefficients for proxies T1 and T2, at two sigma are, respectively, -0.09 ± 0.12 DU year^{-1} and 0.17 ± 0.08 DU year^{-1}. Figure 5 represents the trends before (cyan line) and after (red line) 1997, obtained by the model. According to this figure, the interannual variability of the TOC (blue curve) is well represented by the model (black curve).

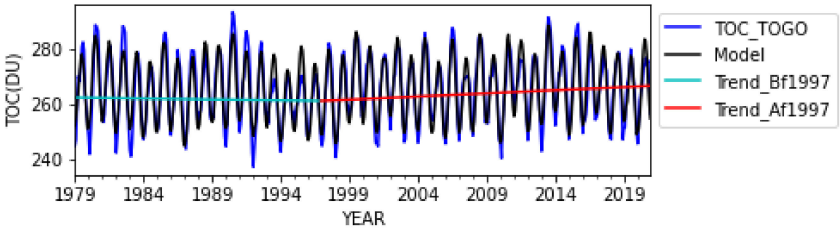

Figure 5. Evolution of the monthly average ozone over Togo observed by MSR-2, simulated by the MLR model, and the trends estimated by the model before and after 1997.

Thus, according to the model, the TOC has a statistically insignificant negative trend before 1997 above Togo. The decrease is a weak value of $0.3\% \pm 0.9\%$ per decade (2σ). After 1997, the trend is positive and statistically significant. The rate of increase is $0.6\% \pm 0.2\%$ per decade (2σ). This trend of close to 1% is different from that obtained in the report of the World Meteorological Organization (WMO) in 2018 [16], which reports that the trends of ozone in the tropical band are almost zero during the period of 1997–2016. This difference of 0.6% could be due to the spatial coverage because this study is limited between 6° N and 11° N, while for the WMO it is a larger region between 20° S and 20° N. Another hypothesis could be related to the temporal coverage of the data used because the time series of the study covered a shorter period. The trend obtained is close to that obtained by Weber et al. [25] from the merged GSG and GTO dataset, where the trend is estimated at $0.3\% \pm 0.3\%$ per decade after 1995 in the tropics at latitudes between 20° and 20° S. It is different from the trends close to zero obtained in the tropics at latitudes between 20° and 20° S after 1995; by the same authors from NASA, NOAA, and WOUDC, who merged the data.

Despite this positive trend estimated after 1997, it is quite small (<1%) and it might not be linked exclusively to the evolution of ozone in the stratosphere and attributed directly to the success of the implementation of the Montreal Protocol. According to Ball et al. [53], the influence of a consequent increase in tropospheric ozone in the tropics may hide an ever-existing decrease in the lower stratosphere. Indeed, a significant decrease

in ozone in the tropics (between 20° S and 20° N) around 35 hPa has been observed by Godin-Beekmann et al. [54], and an increase in tropospheric ozone over the tropics was found [55–58]. Furthermore, the positive value observed for this trend could be related to the cooling of the upper stratosphere resulting from the increase in GHG emissions, which slows the gas phase ozone loss mechanisms in that region (Chapter 5 of the WMO report, 2018) [16]. Thus, a complementary study could be made to elucidate the phenomena of the lower stratosphere using measurements of ozone profiles by satellites above Togo and to study the trend in each layer of the atmosphere to explain the origin of this weak observed trend.

Changes in BDC due to an increase in GHGs emissions [59,60] could diminish the positive trend estimated in this work and make it difficult to detect it linked to the evolution of ODS (CFCs, halons, and HCFCs) since ODS from human activities are still emitted in some parts of the world [61]. This trend should, therefore, be monitored in the coming years.

4.5. Trend by Month

In order to determine the months during which there is a potential recovery of the ozone layer and to make a link between the variability of the TOC and the monsoon and harmattan winds in Togo, the trend for each month was estimated. Table 4 presents the contribution of the different interannual variability forcings, the monthly trend of the TOC since 1997, the adjusted R^2 determination coefficient, and the autocorrelation coefficient. All these results are obtained by applying the Cochrane–Orcutt transformation in the MLR model.

Table 4. Contribution of forcings (QBO30, ENSO, and SF) in the DU and trends after 1997 in the DU year^{-1} for each month. Values are given at 2σ. Bold lines refer to harmattan months while bold and italic lines refer to monsoon months in Togo. Adjusted R^2 represents the percentage of the variability explained by the model after the Cochrane–Orcutt transformation and ρ is the autocorrelation coefficient.

	QBO30 mb	ENSO	SF	Trend	Adjusted R^2	ρ
January	**6.31 ± 0.46**	**−5.54 ± 0.36**	**−0.12 ± 0.60**	**0.07 ± 0.16**	**55%**	**0.20**
February	**5.36 ± 0.46**	**−5.21 ± 0.36**	**1.84 ± 0.64**	**0.08 ± 0.18**	**55%**	**0.00**
March	2.99 ± 0.48	−5.44± 0.36	2.50 ± 0.59	0.20 ± 0.14	64%	0.10
April	2.02 ± 0.53	−5.63 ± 0.36	3.70 ± 0.56	0.10 ± 0.13	68%	0.20
May	2.62± 0.58	−4.49 ± 0.36	4.89 ± 0.53	0.16 ± 0.16	56%	0.10
June	***5.82 ± 0.62***	***−1.62 ± 0.37***	***6.83 ± 0.55***	***0.24 ± 0.20***	***48%***	***0.00***
July	***6.92 ± 0.64***	***1.89 ± 0.37***	***6.04 ± 0.50***	***0.23 ± 0.20***	***54%***	***0.40***
August	***6.31 ± 0.65***	***1.82 ± 0.37***	***6.43 ± 0.58***	***0.31 ± 0.20***	***56%***	***0.00***
September	7.55± 0.63	1.69± 0.37	4.89 ± 0.59	0.28 ± 0.24	55%	0.20
October	7.03 ± 0.62	−1.85 ± 0.37	2.71± 0.60	0.29 ± 0.20	53%	0.30
November	5.97± 0.57	−1.95 ± 0.37	2.59 ± 0.62	0.34 ± 0.16	53%	0.00
December	**5.23 ± 0.51**	**−3.63 ± 0.37**	**1.68 ± 0.65**	**0.12 ± 0.16**	**37%**	**0.10**

According to Table 4 and Figure 6a, trends of ~0.20 DU on average per year are obtained and are statistically significant at 2σ for the periods June–July–August (JJA), September–October–November (SON), and March and May, which correspond to ± 1 month of periods of rain in Togo. The contributions of the QBO30 and the ENSO are significant throughout the year. As for the Solar Flux, its contribution is significant throughout the year, except during the month of January (Figure 6b). These trends observed in the rainy season are higher than in other periods and could be due to the fact that during this season there is the mechanism of low pressure and lower tropopause height, which may contribute

to an increase in the TOC [62], in addition to the possible ODS decrease in the stratosphere. Moreover, it could probably be related to the NOx generated by lightning NOx (LNOx) during the rainy season, which contributes to the photochemical production of ozone in the upper tropospheric–lower stratospheric layer [63]. The same relationship between the TOC trend and NOx was established in the work of Toihir et al. [34] to explain the strong TOC trend observed at the Bauru site. This possible contribution needs to be further investigated.

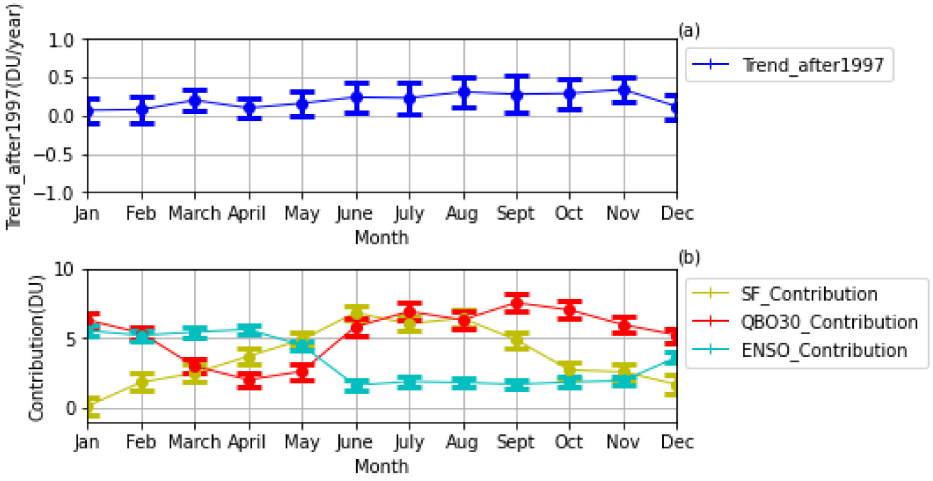

Figure 6. The trend in the variability of ozone per month (2σ) in Togo after 1997 (**a**), the seasonal contribution of the forcings (**b**).

Finally, from this part of the work, it is to be concluded that the monthly trend of the TOC is positive and significant in the rainy season (particularly in the monsoon period) except in April, but it is not significant in the harmattan period.

5. Conclusions

This work, which is a contribution to the observation of the total ozone column, is the first study that targets the evolution of ozone above Togo, with an analysis of the long-term and interannual variability of the ozone total content. It has quantified the influence of the different forcings on the interannual variability of the TOC. The set of standard proxies considered in this study presented a significant contribution at >2 σ, except the QBO10 and the SAnO. In addition, the study quantified the trends before and after the year of the peak of the EESC in the stratosphere in 1997. Thus, before the year of the peak, the trend is weak and statistically insignificant. After the year of the peak, a statistically significant positive trend is observed which cannot be directly associated with the success of the implementation of the Montreal Protocol. The recovery rate of the total ozone column is 0.6% ± 0.2% per decade which, therefore, shows a smaller increase in total ozone column above Togo compared to the extra areas tropical regions where the rate is above 1% (1.74% ± 0.40%), according to the work of Toihir et al. [34]. It is possible that this weak trend obtained is due to certain factors, such as a decrease in ozone at 35 hPa [54] and an increase in tropospheric ozone over the tropics [55–58]. Thanks to this study, it was also shown that the variability of the TOC during the year is positive and significant in the rainy months, except for April. From the perspectives gained by this work, a complementary study could be made to elucidate the phenomena of the lower stratosphere above Togo to study the trend in each layer of the atmosphere and the factors which can influence the TOC in the rainy season above Togo.

Author Contributions: Conceptualization, K.A., A.P. and K.S.; methodology, K.A. and K.S.; software, A.B.; validation, A.P., K.S. and S.G.-B.; formal analysis and investigation, K.A.; resources, A.P.; data curation, A.B.; writing original draft preparation, K.A.; writing review, editing, and supervision A.P.; visualization, K.A., A.P. and K.S. All authors have read and agreed to the published version of the manuscript.

Funding: The APC was funded by CAMS27/Copernicus. K.A. has been a beneficiary of the 6 months Campus France SCAC Scholarship.

Institutional Review Board Statement: Not applicable.

Data Availability Statement: The data collected are monthly average values and cover 1979–2020. These data cover the national territory with latitudes between 6° and 11° N, and longitudes between 0°14′ W and 1°65′ E. They were downloaded from the website of the tropospheric emissions monitoring service (TEMIS) of KNMI/ESA at the following address: https://www.temis.nl/protocols/o3total.php (accessed on 17 September 2021).

Acknowledgments: This work was carried out thanks to the scholarship funded by the Cooperation and Cultural Action Service of the French Embassy (SCAC) in Togo; so, the authors warmly thank the SCAC and Campus France which is the executing organization of the scholarship.

Conflicts of Interest: The authors declare that they have no conflict of interest.

Appendix A

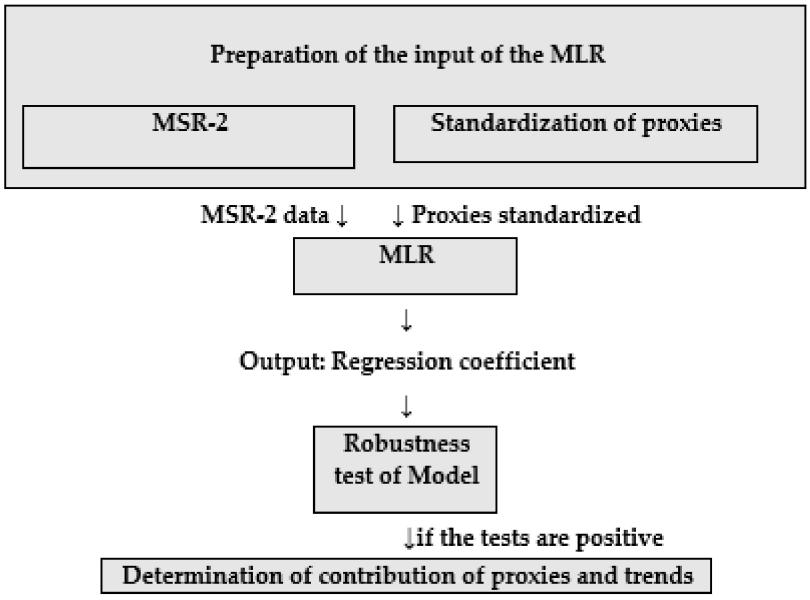

Figure A1. Flow chart of the methodology applied.

References

1. McMichael, A.J.; Haines, J.A.; Slooff, R.; Sari Kovats, R.; World Health Organization. *Climate Change and Human Health: An Assessment*; No. WHO/EHG/96.7; World Health Organization: Geneva, Switzerland, 1996.
2. Kakani, V.G.; Reddy, K.R.; Zhao, D.; Sailaja, K. Field crop responses to ultraviolet-B radiation: A review. *Agric. For. Meteorol.* **2003**, *120*, 191–218. [CrossRef]
3. Vernet, M.; Brody, E.A.; Holm-Hansen, O.; Mitchell, B.G. The response of Antarctic phytoplankton to ultraviolet radiation: Absorption, photosynthesis, and taxonomic composition. In *Ultraviolet Radiation in Antarctica: Measurements and Biological Effects*; Weiler, C.S., Penhale, P.A., Eds.; American Geophysical Union: Washington, DC, USA, 1994; pp. 143–158.
4. Butchart, N. The Brewer-Dobson circulation. *Rev. Geophys.* **2014**, *52*, 157–184. [CrossRef]
5. Harris, N.R.; Kyrö, E.; Staehelin, J.; Brunner, D.; Andersen, S.-B.; Godin-Beekmann, S.; Dhomse, S.; Hadjinicolaou, P.; Hansen, G.; Isaksen, I.; et al. Ozone trends at northern mid- and high latitudes—A European perspective. *Geophys. Ann.* **2008**, *26*, 1207–1220. [CrossRef]
6. Weber, M.; Dikty, S.; Burrows, J.; Garny, H.; Dameris, M.; Kubin, A.; Abalichin, J.; Langematz, U. The Brewer-Dobson circulation and total ozone from seasonal to decacadal time scale. *Atmos. Chem. Phys.* **2011**, *11*, 11221–11235. [CrossRef]

7. Montzka, S.; Reimannander, S.; Engel, A.; Kruger, K.; Simon, O.; Sturges, W.; Blake, D.; Dorf, M.; Fraser, P.; Froidevaux, L.; et al. Ozone-Depleting Substances (ODSs) and Related Chemicals, Chapter 1. In *Scientific Assessment of Ozone Depletion: 2010, Global Ozone Research and Monitoring Project-Report No.52*; World Meteorological Organization: Geneva, Switzerland, 2011. Available online: https://tsapps.nist.gov/publication/get_pdf.cfm?pub_id=909747 (accessed on 4 December 2022).
8. Kuttippurath, J.; Lefèvre, F.; Pommereau, J.; Roscoe, H.K.; Goutail, F.; Pazmiño, A.; Shanklin, J.D. Antarctic ozone loss in 1979–2010: First sign of ozone recovery. *Atmos. Chem. Phys.* **2013**, *13*, 1625–1635. [CrossRef]
9. Krzyścin, W.J.; Baranowski, D.B. Signs of the ozone recovery based on multi sensor reanalysis of total ozone for the period 1979–2017. *Atmos. Environ.* **2019**, *199*, 334–344. [CrossRef]
10. Reinsel, G.C.; Miller, A.J.; Weatherhead, E.C.; Flynn, L.E.; Nagatani, R.M.; Tiao, G.C.; Wuebbles, D.J. Trend analysis of total ozone data for turnaround and dynamical contributions. *J. Geophys. Res.* **2005**, *110*, D16306. [CrossRef]
11. Farman, J.; Gardiner, B.; Shanklin, J. Large losses of total ozone in Antarctica reveal seasonal ClOx/NOx interaction. *Nature* **1985**, *315*, 207–210. [CrossRef]
12. World Meteorological Organization (WMO). *Scientific Assessment of Ozone Depletion: 2014*; World Meteorological Organization (WMO): Geneva, Switzerland, 2014.
13. Solomon, S.; Garcia, R.; Rowland, F.; Donald, J. On the depletion of Antarctic ozone. *Nature* **1986**, *321*, 755–758. [CrossRef]
14. McElroy, M.; Salawitch, R.; Wofsy, S.; Logan, J. Reductions of Antarctic ozone due to synergistic interactions of chlorine and bromine. *Nature* **1986**, *321*, 759–762. [CrossRef]
15. UNEP. *Handbook for the Montreal Protocol on Substances that Deplete the Ozone Layer*, 13th ed.; Ozone Secretariat: Nairobi, Kenya, 2019.
16. WMO (World Meteorological Organization). *Scientific Assessment of Ozone Depletion: 2018, Global Ozone Research and Monitoring*; Project-Report No.58; WMO (World Meteorological Organization): Geneva, Switzerland, 2018.
17. Klobas, J.E.; Weisenstein, D.K.; Salawitch, R.J.; Wilmouth, D.M. Reformulating the bromine alpha factor and equivalent effective stratospheric chlorine (EESC): Evolution of ozone destruction rates of bromine and chlorine in future climate scenarios. *Atmos. Chem. Phys.* **2020**, *20*, 9459–9471. [CrossRef]
18. Newman, A.; Daniel, J.S.; Waugh, D.W.; Nash, E.R. A new formulation of equivalent effective stratospheric chlorine (EESC). Atmos. *Chem. Phys.* **2007**, *7*, 3963–4000.
19. Braesicke, P.; Neu, J.L.; Fioletov, V.E.; Godin-Beekmann, S.; Hubert, D.; Petropavlovskikh, I.; Shiotani, M.; Sinnhuber, B.M.; Ball, W.; Chang, K.L.; et al. Update on Global Ozone: Past, Present, and Future, Chapter 3. In *WMO Scientific Assessment of Ozone Depletion (2018)*; WMO: Geneva, Switzerland, 2018; Volume 58.
20. Ball, W.T.; Alsing, J.; Mortlock, D.J.; Staehelin, J.; Haigh, J.D.; Peter, T.; Tummon, F.; Stübi, R.; Stenke, A.; Anderson, J.; et al. Evidence for a continuous decline in lower stratospheric ozone offsetting ozone layer recovery. *Atmos. Chem. Phys.* **2018**, *18*, 1379–1394. [CrossRef]
21. Smyshlyaev, S.; Galin, V.Y.; Blakitnaya, A.; Jakovlev, A.R. Numerical Modeling of the Natural and Manmade Factors Influencing Past and Current Changes in Polar, and Tropical Ozone. *Atmosphere* **2020**, *11*, 76. [CrossRef]
22. Coldewey-Egbers, M.; Loyola, D.G.; Lerot, C.; Roozendael, M.V. Global, regional and seasonal analysis of total ozone trends derived from the 1995–2020 GTO-ECV climate data record. *Atmos. Chem. Phys.* **2022**, *22*, 6861–6878. [CrossRef]
23. Meul, S.; Dameris, M.; Langematz, U.; Abalichin, J.; Kerschbaumer, A.; Kubin, A.; Oberländer-Hayn, S. Impact of rising greenhouse gas concentrations on future tropical ozone and UV exposure. Geophys. *Res. Lett.* **2016**, *43*, 2919–2927. [CrossRef]
24. Szeląg, M.E.; Sofieva, V.F.; Degenstein, D.; Roth, C.; Davis, S.; Froidevaux, L. Seasonal stratospheric ozone trends over 2000–2018 derived from several merged data sets. *Atmos. Chem. Phys.* **2020**, *20*, 7035–7704.
25. Weber, M.; Arosio, C.; Coldewey-Egbers, M.; Fioletov, V.E.; Frith, S.M.; Wild, J.D.; Tourpali, K.; Burrows, J.; Loyola, D. Global total ozone recovery trends attributed to ozone-depleting substance (ODS) changes derived from. *Atmos. Chem. Phys.* **2022**, *22*, 6843–6859. [CrossRef]
26. Ramaswamy, V.; Schwarzkopf, M.D.; Randel, W.J.; Santer, B.D.; Soden, B.J.; Stenchikov, G.L. Anthropogenic and natural influences in the evolution of lower stratospheric cooling. *Science* **2006**, *311*, 1138–1141. [CrossRef]
27. Bencherif, H.; Toihir, A.; Mbatha, N.; Sivakumar, V.; du Preez, D.; Bègue, N.; Coetzee, G. Ozone Variability and Trend Estimates from 20-Yearsof Ground-Based and Satellite Observations at Irene Station, South Africa. *Atmosphere* **2020**, *11*, 1216. [CrossRef]
28. Pazmiño, A.; Godin-Beekmann, S.; Hauchecorne, A.; Claud, C.; Khaykin, S. Multiple symptoms of total ozone recovery inside the Antarctic. Atmos. *Chem. Phys.* **2018**, *18*, 7557–7572.
29. Nair, J.; Godin-Beekmann, S.; Kuttippurath, J.; Ancellet, G.; Goutail, F.; Pazmiño, A.; Froidevaux, L.; Zawodny, J.M.; Evans, R.D.; Wang, H.J.; et al. Ozone trends derived from the total column and vertical profiles at a northern mid-latitude station. *Atmos. Chem. Phys.* **2013**, *13*, 7081–7112. [CrossRef]
30. Van Der A, R.J.; Allaart, M.A.F.; Eskes, H.J. Multi sensor re-analysis of total ozone. *Atmos. Chem. Phys.* **2010**, *10*, 11277–11294. [CrossRef]
31. Van Der A, R.J.; Allaart, M.A.F.; Eskes, H.J. Extended and refined multi sensor reanalysis of total ozone for the period 1970–2012. *Atmos. Meas. Tech.* **2015**, *8*, 3021–3035. [CrossRef]
32. R Core Team (2022) R: A Language and Environment for Statistical Computing; R Foundation for Statistical Computing: Vienna, Austria. Available online: https://www.R-project.org/ (accessed on 16 August 2022).
33. Tiao, G.; Reinse, G.; Xu, D.; Pedrick, J.; Zhu, X.; Miller, A.; Deluis, I.J.; Mateer, C.; Wuebbles, D. Effects of correlation and temporal sampling schemes on estimates of trend and spatial correlation. *J. Geophys. Res.* **1990**, *95*, 507–517. [CrossRef]

34. Toihir, A.M.; Portafaix, T.; Sivakumar, V.; Bencherif, H.; Pazmino, A.; Bègue, N. Variability and trend in ozone over the southern tropics and subtropics. *Ann. Geophys.* **2018**, *36*, 381–404. [CrossRef]
35. Olsen, M.A.; Manney, G.L.; Liu, J. The ENSO and QBO impact on ozone variability and stratosphere-Troposphere exchange relative to the subtropical jets. *J. Geophys. Res. Atmos.* **2019**, *124*, 7379–7392. [CrossRef]
36. Han, Z.; Chongping, J.; Libo, Z. QBO Signal in total ozone over Tibet. *Adv. Atmos. Sci.* **2000**, *17*, 562–568. [CrossRef]
37. Chehade, W.; Weber, M.; Burrows, J.P. Total ozone trends and variability during 1979–2012 from merged data sets of various satellites. *Atmos. Chem. Phys.* **2014**, *14*, 7059–7074. [CrossRef]
38. Jin, D.; Kirtman, B. The impact of ENSO periodicity on North Pacific SST variability. *Clim. Dyn.* **2010**, *34*, 1015–1039. [CrossRef]
39. Dijkstra, H.A. The ENSO phenomenon: Theory and mechanisms. *Adv. Goesci.* **2006**, *6*, 3–15. [CrossRef]
40. Shiotani, M. Annual, quasi-biennial, and El Nino-Southern Oscillation (ENSO) time-scale variations in equatorial total ozone. *J. Geophys. Res.* **1992**, *97*, 7625–7633. [CrossRef]
41. Randel, W.J.; Garcia, R.R.; Calvo, N.; Marsh, D. ENSO influence on zonal mean temperature and ozone in the tropicallower stratosphere. *Geophys. Res. Lett.* **2009**, *36*, L15822. [CrossRef]
42. Bourassa, A.E.; Degenstein, D.A.; Randel, W.J.; Zawodny, J.M.; Kyrölä, E.; McLinden, C.A.; Sioris, C.E.; Roth, C.Z. Trends in stratospheric ozone derived from merged SAGE II and Odin-OSIRIS satellite observations. *Atmos. Chem. Phys.* **2014**, *14*, 6983–6994. [CrossRef]
43. Li, K.-F.; Jiang, X.; Liang, M.-C.; Yun, Y.L. Simulation of solar-cycle response in tropical total column ozone using. *Atmos. Chem. Phys.* **2012**, *12*, 1867–1893.
44. Bojkov, R.D.; Fioletov, V.E. Total ozone variations in the tropical belt: An application for quality of ground based measurements. *Mefeorology Atmos. Phys.* **1996**, *58*, 223–240. [CrossRef]
45. Labitzke, K. The global signal of the 11-year solar cycle in the stratosphere: Observations and models: Differences between solar maxima and minima. *Meteorol. Z.* **2001**, *10*, 83–90. [CrossRef]
46. Gray, L.J.; Beer, J.; Geller, M.; Haigh, J.D.; Lockwood, M.; Matthes, K.; Cubasch, U. Solar influences on climate. *Rev. Geophys.* **2010**, *48*, 2010. [CrossRef]
47. Soukharev, B.E.; Hood, L.L. Solar cycle variation of stratospheric ozone: Multiple regression analysis of long-term satellite data sets and comparisons with models. *J. Geophys. Res.* **2006**, *111*, D20314. [CrossRef]
48. Reinsel, G.C.; Weatherhead, E.; Tiao, G.C.; Miller, A.J.; Nagatani, R.M.; Wuebbles, D.J.; Flynn, L.E. On detection of turnaround and recovery in trend of ozone. *J. Geophys.* **2002**, *107*, 4078. [CrossRef]
49. Petropavlovskikh, I.; Godin-Beekmann, S.; Hubert, D.; Damadeo, R.; Hassler, B.; Sofieva, V. SPARC/IO3C/GAW Report on Long-term Ozone Trends and Uncertainties in the Stratosphere. PARC/IO3C/GAW, 2019: SPARC Report No. 9, GAW Report No. 241, WCRP-17/2018. Available online: www.sparc-climate.org/publications/sparc-reports (accessed on 11 November 2022).
50. Steinbrecht, W.; Hassler, B.; Claude, H.; Winkler, P.; Stolarski, R.S. Global distribution of total ozone and lower stratospheric temperature variations. *Atmos. Chem. Phys.* **2003**, *3*, 1421–1438. [CrossRef]
51. Zerefos, C.S.; Bais, A.F.; Ziomas, I.C.; Bojkov, R.D. On the relative importance of Quasi-Biennial Oscillation and El Ni ño/Southern Oscillation in the Revised Dobson Total Ozone Records. *J. Geophys. Res.* **1992**, *97*, 10135–10144. [CrossRef]
52. Poulain, V.; Bekki, S.; Marchand, M.; Chipperfield, M.; Khodri, M.; Lefèvre, F.; Dhomse, S. Evaluation of the Inter-Annual Variability of Stratospheric Chemical Composition in Chemistry-Climate Models Using Ground-Based Multi Species Time. *J. Atmos. Sol. Terr. Phys.* **2016**, *145*, 61–84. [CrossRef]
53. Ball, W.T. (QOS) Evidence that tropical total column ozone no longer represents stratospheric changes. Personal communication, 2021.
54. Godin-Beekmann, S.; Azouz, N.; Sofieva, V.; Hubert, D.; Petropavlovskikh, I.; Effertz, P.; Ancellet, G.; Degenstein, D.A.; Zawada, D.; Froidevaux, L.; et al. Updated trends of thozone vertical distribution in the in the 60° S–60° N latitude range based an LOTUS regression model. *Atmos. Chem. Phys.* **2022**, *22*, 11657–11673. [CrossRef]
55. Thompson, A.M.; Stauffer, R.M.; Wargan, K.; Witte, J.C.; Kollonige, D.E.; Ziemke, J.R. Regional and Seasonal Trends in Tropical Ozone From SHADOZ Profiles: Reference for Models and Satellite Products. *J. Geophys. Res. Atmos.* **2021**, *126*, e2021JD034691. [CrossRef]
56. Leventidou, E.; Weber, M.; Eichmann, K.-U.; Burrows, J.; Heue, K.; Thompson, A.M. Harmonisation and trends of 20-year tropical tropospheric ozone data. *Atmos. Chem. Phys.* **2018**, *18*, 9189–9205. [CrossRef]
57. Gaudel, A.; Cooper, O.R.; Ancellet, G.; Barret, B.; Boynard, A.; Burrows, J.; Clerbaux, C.; Coheur, P.-F.; Cuesta, J.; Cuevas, E.; et al. Tropospheric Ozone Assessment Report: Present-day distribution and trends of tropospheric ozone relevant to climate and global atmospheric chemistry model evaluation. *Elem. Sci. Anthr.* **2018**, *6*, 39. [CrossRef]
58. Tarasick, D.; Galbally, I.E.; Cooper, O.R.; Schultz, M.G.; Ancellet, G.; Leblanc, T.; Wallington, T.J.; Ziemke, J.; Liu, X.; Steinbacher, M.; et al. Tropospheric Ozone Assessment Report: Tropospheric ozone from 1877 to 2016, observed levels, trends and uncertainties. *Elem. Sci. Anthr.* **2019**, *7*, 39. [CrossRef]
59. Butchart, N.; Scaife, A.; Bourqui, M.; Grandpré, J.d.; Hare, S.; Kettleborough, J.; Langematz, U.; Manzini, E.; Sassi, F.; Shibata, K.; et al. Simulations of anthropogenic change in the strength of the Brewer-Dobson circulation. *Clim. Dyn.* **2006**, *27*, 727–741. [CrossRef]

60. Eyring, V.; Shepherd, T.; Waugh, D., Eds. SPARC, 2010: SPARC CCMVal Report on the Evaluation of Chemistry-Climate Models. SPARC Report No. 5, WCRP-30/2010, WMO/TD—No. 40. Available online: www.sparc-climate.org/publications/sparc-reports/ (accessed on 4 December 2022).
61. Montzka, S.; Dutton, G.; Yu, P.; Ray, E.; Portmann, R.W.; Daniel, J.S.; Kuijpers, L.; Hall, B.D.; Mondeel, D.; Siso, C.; et al. An unexpected and persistent increase in global emissions of ozone-depleting CFC-11. *Nature* **2018**, *557*, 413–417. [CrossRef]
62. Okoro, E.; Okeke, F.; Omeje, L. Investigating Contributions of Total Column Ozone Variation on Some Meteorological Parameters in Nigeria. *Atmos. Clim. Sci.* **2022**, *12*, 132–149. [CrossRef]
63. Verma, S.; Yadava, P.K.; Lal, D.M.; Mall, R.K.; Kumar, H.; Payra, S. Role of Lightning NOx in Ozone Formation: A Review. *Pure Appl. Geophys.* **2021**, *178*, 1425–1443. [CrossRef]